Automated Color Balance and Contrast Enhancement of Retinal Images for Visual Diagnosis

P. Vonghirandecha, M. Karnjanadecha and S. Intajag

***Abstract*—**Color retinal image enhancement plays an important role in creating an image suitable for medical diagnosis for the early detection of eye disease. For this problem domain, we propose histogram-based color balance and contrast enhancement (CBCE) which automatically adjusts the intensity values under psychometric constraints by employing generalized extreme value functions. The results show that our algorithm performs color retinal image enhancement well, while retaining a pleasing natural appearance for visually diagnosing the image. The performance of our method has been evaluated against data from the Structured Analysis of the Retina and the Diabetic Retinopathy image databases.

***Keywords*—**Histogram specification, generalized extreme value, retinal images, color balance, psychometric function.

I. INTRODUCTION

MANY eye diseases, including age-related macular degeneration (AMD) and diabetic retinopathy [1] [2], manifest themselves in the retina, and some are the leading causes of blindness. As a consequence, retinal images are widely used by ophthalmologists to identify patients who may be at risk from eye disease. However, those images may be unsuitable for diagnosis due to their poor quality, caused by non-uniform illumination, low contrast, or washed-out color [3] [4]. Such images need to be enhanced to provide better visibility of the retinal anatomical structures.

We propose an improvement to previously exiting algorithms in order to allow physicians to more easily and accurately diagnose the disease.

Image processing algorithms for improving the poor quality images include decomposition techniques [5] which decompose an image into high and low frequency signals then process the two signals, and histogram specification techniques [6] [7]. The histogram specification techniques modify the image by creating a pixel mapping function, and use it to redistribute the original image histogram to increase the image's contrast. These techniques have received the most attention due to their straightforward and intuitive implementation.

For decomposition technique, Dai *et al*. [5] proposed retinal fundus image enhancement using normalized convolution and noise removal. The information in the background image was extracted from the original image by applying a normalized convolution algorithm [8]. In order to obtain an enhanced image, the difference between the original image and the background image was multiplied by a contrast factor, and fused with the original image. The fused image was de-noised by applying fourth-order partial differential equations [9] and a relaxed median filter [10]. This technique can reduce abrupt changes and improve detailed information by increasing the image contrast, especially in the region of retinal vessels. However, this decomposition technique is a complex computations.

For histogram-based methods, histogram equalization (HE) is widely used to enhance the contrast of grey-scale images, by employing a cumulative distribution function (CDF) to stretch their dynamic range. However, for a color image, HE may produce unwanted artefacts, color imbalance, loss of detail, and it may shift the mean intensity values to the middle of the intensity range. Many algorithms have been proposed with various constraints, such as brightness preservation [11] [12] [13] and contrast limitation [14]. However, brightness preservation algorithms provide output images with a mean brightness close to the original, which is inappropriate for under-exposed or over-exposed images; especially, a color retinal photograph. In addition, the contrast-limited adaptive histogram equalization (CLAHE) algorithm [15] is disadvantageous as it is difficult to determine many of the parameters, such as clip limit, tile size, and mapping functions. It is generally only used to enhance the luminance channel.

A color retinal image enhancement based on luminosity and contrast adjustment [6] has been proposed, which augments the classical histogram equalization. In this method, the R, G, and B channels are enhanced by a luminance gain matrix, which is obtained by gamma correction of the value channel, V, in hue-saturation-value (HSV) color space. The contrast of the luminosity channel of L*a*b can be further enhanced by applying the CLAHE method with the number of tiles and the clip limit equal to 8×8 and 0.01, respectively.

This work was supported by Prince of Songkla University Grant no. SCI600372S.

P. Vonghirandecha is with the Department of Computer Engineering, Faculty of Engineering, Prince of Songkla University, Songkhla, Thailand. (e-mail: preecha.v@psu.ac.th).

M. Karnjanadecha is with the Department of Computer Engineering, Faculty of Engineering, Prince of Songkla University, Songkhla, Thailand. (e-mail: montri@coe.psu.ac.th).

S. Intajag is with the Department of Computer Science, Faculty of Science, Prince of Songkla University, Songkhla, Thailand. (e-mail: sathit.i@psu.ac.th).

The methods set out above deal with brightness and contrast enhancement, but they do not adjust the color balance to improve the color image quality. Intajag *et al*. [7] proposed a histogram specification method with generalized extreme value distribution (HS-GEV), to automatically adjust the brightness, contrast, and color balance by redistributing the image data. This was utilized to support the population screening of AMD lesions.

In order to improve the retinal color images, our method automatically enhances the images by modifying HS-GEV [7] to increase the contrast and color balance, while preserving naturalness, and taking into consideration the human visual system. Our algorithm uses a contrast sensitivity function (CSF) [16] to develop a criterion for justifying the image quality. The specifications of the enhanced images are designed according to optimal standardized images provided by the AREDS2 Reading Center [3]. The performance of our method was evaluated using two publicly available datasets, Structured Analysis of the Retina (STARE) [17] and the Diabetic Retinopathy Database (DIARETDB0) [18]. The results show that our algorithm can make the interesting parts of retinal images more visible, and these enhanced images could help ophthalmologists during disease diagnostic procedures.

This paper proceeds as follows: the image databases are introduced in section II-A, and section II-B summarizes histogram specification, GEV distribution, probability weighted moment (PWM) estimation, and HS-GEV. Section III describes our algorithm in detail. Our experimental results appear in section IV, and conclusions in section V.

II. Materials and Basic Theory

A. Materials

We employ two publicly available datasets: Structured Analysis of the Retina [17], and the Diabetic Retinopathy Database [18], to evaluate the performance of our method. The STARE dataset, acquired by Hoover *et al.* [17], consists of 36 normal and 47 AMD images. The images were taken with a 35° field of view, and each occupies 700×605 pixels, and are stored in 24-bit PPM format. The DIARETDB0 database, acquired by Kauppi *et al*. [18], consists of 20 normal images and 110 containing signs of diabetic retinopathy. The images were taken with a 50° field of view, are 1500×1152 pixels large, and stored in 24-bit PNG format.

B. Basic theory

The proposed method incorporates histogram specification (HS) with support from GEV distribution and parameter estimation using the PWM method. Also, the retinal image enhancement employs HS-GEV. The rest of this sub-section gives some background on these four techniques.

B.1. Histogram Specification

Histogram equalization employs the probability density function (PDF) and the cumulative distribution function [19] to achieve a uniform distribution in image processing. HE can usually produce good quality image contrast when the image has approximately a uniform distribution.

Let r denote the grey levels of the input image to be enhanced. Assume that r is a continuous random variable which has been normalized in the range [0, 1] and its continuous probability density function is $p_r(r)$. Suppose $T(r)=\int_{-\infty}^{r} p_r(w)\,dw$ is the CDF of *r*, which is strictly increasing; therefore, *T*(*r*) is uniformly distributed in [0, 1].

For a grey level image, its intensity value is a discrete integer in the range [0, *L*-1] (where *L* denotes the maximum number of intensity values). Hence (*L*-1) × *T*(*r*) will be uniform in [0, *L*-1] and the transform $r \rightarrow (L\text{-}1) \times T(r)$ is an equalization of the grey level image [19] [20]. A transformation function that produces an output intensity level *z* by histogram equalization has the form:

$$z=(L-1)T(r)=(L-1)\int_{-\infty}^{r} p_r(w)\,dw, \qquad (1)$$

where *w* is a dummy variable of integration.

Histogram equalization yields an image whose pixels are uniformly distributed among all the grey levels. However, the intensity values of retinal images typically have more complex distributions than uniform, which mean that HE may not be appropriate. In general, retinal image enhancement uses not only a scaling parameter to increase the image contrast, but also employs the centroid density and shape parameter for the frequency distributions to specify the color balance and to map color tone. Histogram specification addresses this issue by letting us specify the optimal distribution. Let, *g* represent the output intensity levels of the desired image, and $p_g(g)$ be the specified PDF. Pratt [21] defined the specifying function as:

$$H(g)=(L-1)\int_{-\infty}^{g} p_g(u)\,du=z, \qquad (2)$$

where *u* is a dummy variable of integration. From equations (1) and (2), the output intensity level, *g* of the desired image becomes:

$$g=H^{-1}(z), \qquad (3)$$

where H^{-1} is an inverse transformation function that maps grey-scale values in the input image to the desired image. More detailed information of histogram specification can be found in Gonzalez *et al*. [19].

The specified histogram, $p_g(g)$ can be used by many types of probability function [21], such as uniform, hyperbolic, exponential, and Rayleigh distributions. These PDFs usually enhance monochrome images by controlling the range or shape parameters. In order to specify the histogram of a color image, a GEV distribution is employed, consisting of

shape, scale, and location parameters. This provides control over the shape, range, and brightness location.

B.2. Generalized Extreme Value

The extreme value theory by Fisher and Tippet [22] is a cornerstone of distribution functions, and a good review of GEV applications appears in Fararo and Katz [23]. The CDF of a GEV [24] is given by:

$$y = F(x) = \begin{cases} \exp\left\{-\left[1-\kappa\frac{(x-\mu)}{\sigma}\right]^{1/\kappa}\right\}, \\ \qquad \kappa\neq 0, \begin{cases} \mu+\sigma/\kappa \le x < \infty, \text{ for } \kappa<0; \\ -\infty < x \le \mu+\sigma/\kappa, \text{ for } \kappa>0; \end{cases} \\ \exp\left\{-\exp\left[-\frac{(x-\mu)}{\sigma}\right]\right\}, \quad -\infty<x<\infty, \text{ for } \kappa=0. \end{cases} \tag{4}$$

The GEV distribution includes three parameters: the location (μ) which determines the mode of the GEV distribution, the scale (σ) which specifies the deviation, and the shape (κ) which indicates how rapidly the upper tail decays. Three types of distribution can be determined by the κ value. Negative κ is a Type III or Weibull distribution, which has a bound tail. Positive κ is a Type II or Frechet distribution, which has a heavy tail. When κ approaches zero, it becomes a Type I or Gumbel distribution, which displays an exponential tail.

In our work, the three GEV parameters are used to adjust the brightness, contrast, and color balance of the color images. The PDF corresponding to (4) is:

$$f(x) = \begin{cases} \exp\left\{-\left(1+\kappa(x-\mu)/\sigma\right)^{-1/\kappa}\right\}\frac{1}{\sigma}\left[1+\kappa\left(\frac{x-\mu}{\sigma}\right)\right]^{-\frac{1}{\kappa}-1} \\ \qquad \begin{cases} \mu+\sigma/\kappa \le x < \infty, \text{ for } \kappa<0; \\ -\infty < x \le \mu+\sigma/\kappa, \text{ for } \kappa>0; \end{cases} \\ \exp\left\{-\exp\left[-\frac{(x-\mu)}{\sigma}\right]\right\}\frac{1}{\sigma}\exp\left[-\frac{(x-\mu)}{\sigma}\right], \ -\infty<x<\infty, \text{ for } \kappa=0. \end{cases} \tag{5}$$

Since the cumulative distribution function is invertible, it can be expressed in the form:

$$x = F^{-1}(y) = \begin{cases} \mu+\frac{\sigma}{\kappa}\left[1-(-\ln y)^{\kappa}\right] & \text{for } \kappa\neq 0; \\ \mu-\sigma\ln(-\ln y) & \text{for } \kappa=0. \end{cases} \tag{6}$$

To design the HS using a GEV distribution, the inverse function, H^{-1} in (3) can be represented by the inverse function, F^{-1} in (6) to generate the specified intensity, *g*. This means that the transfer function for the HS based on the GEV distribution becomes:

$$g = H^{-1}(z) = \begin{cases} \mu+\frac{\sigma}{\kappa}\left[1-(-\ln z)^{\kappa}\right] & \text{for } \kappa\neq 0; \\ \mu-\sigma\ln(-\ln z) & \text{for } \kappa=0. \end{cases} \tag{7}$$

In other words, the image enhancement quality of the HS now depends on designing suitable GEV parameters. These can be estimated by the PWM method.

B.3. Probability weighted moments

The μ, σ, and κ parameters of the GEV can be reliably estimated using the PWMs described by Hosking *et al*. [25]:

$$\hat{\kappa} = 7.8590c + 2.9554c^2, \tag{8}$$

$$\hat{\sigma} = \frac{(2b_1-b_0)\hat{\kappa}}{\left(1-2^{-\hat{\kappa}}\right)\Gamma\left(1+\hat{\kappa}\right)}, \tag{9}$$

$$\hat{\mu} = b_0 - \frac{\hat{\sigma}}{\hat{\kappa}}\left[1-\Gamma\left(1+\hat{\kappa}\right)\right], \tag{10}$$

where $c = (2b_1 - b_0)/(3b_2 - b_0) - \log 2/\log 3$, and Γ denotes a gamma function. The values, b_0, b_1, and b_2 are calculated by employing an unbiased estimator of the first three PWMs, given by:

$$b_r = \sum_{i=1}^{n}\frac{(i-1)(i-2)(i-3)\ldots(i-r)}{n(n-1)(n-2)(n-3)\ldots(n-r)}x_{(i)}, \quad r = 0,1,2,\ldots \tag{11}$$

where $x_{(i)}$ denotes the ordered observations from a sample of size *n*, that is $\left\{x_{(1)} \le x_{(2)} \le x_{(3)} \le \ldots \le x_{(n)}\right\}$.

B.4. Retinal image enhancement by HS-GEV

The HS-GEV model [7] employs a generalized extreme value distribution [24] [26] to design the transfer functions of the histogram specification technique [19] [21] [27]. The transfer functions are specified with three GEV parameters to control the brightness, contrast, and color balance of the retinal images. These parameters consist of shape, scale, and location, which are estimated by PWMs as outlined above.

HS-GEV uses Kullback–Leibler divergence (KLD) [28] to find the optimal GEV parameters in an iterative process, which consists of two loops of shape and scale parameters. Each shape parameter is used to adjust the tone, while the scale parameter is used to increase the dynamic range. In each iteration, the location parameter is recalculated to update the KLD values as seen in the sequence of the equations (8)-(10). Although HS-GEV could be employed to effectively enhance color retinal images, optimal GEV parameters with maximized KLD values could generate darker or brighter regions, as illustrated by column (b) of Fig. 1.

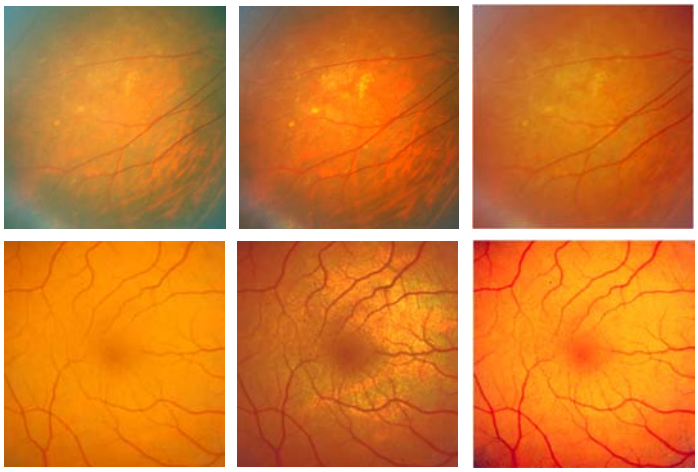

(a) (b) (c)

Fig. 1 Comparison enhancement results by columns: (a) Original images from files im0292.ppm, and im0082.ppm, (b) Enhanced images by HS-GEV, (c) Enhanced images by our method.

Our algorithm, color balance and contrast enhancement (CBCE), is proposed to overcome some drawbacks of the HS-GEV method as illustrated by a comparison of the image results in columns (b) and (c) of Fig. 1. The purpose of this improvement, and the main contribution of our work, is to provide a good quality fundus image, as seen in the column (c); we replace the cost function, KLD of HS-GEV with an achromatic contrast sensitivity quality metric (ACSQM), and compensate for non-uniform illumination as seen in the flow diagram of CBCE in Fig. 2.

The CBCE diagram is comprised of two main parts. The first initializes the process variables and estimates the GEV parameters of the input image. The second part is an iterative process to find the optimal GEV parameters by assessing the image quality index.

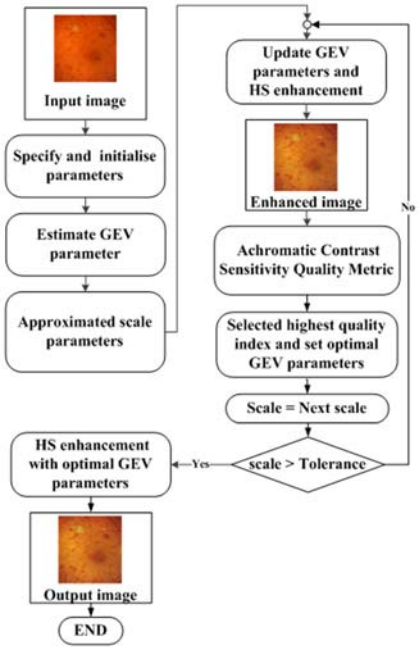

Fig. 2 Flow diagram of our method.

III. Color Retinal Image Enhancement Method

Our method enhances color retinal images to be optimal for human diagnosis. This requires that we extend the CBCE algorithm from the HS-GEV method to deal with the problems illustrated in Fig. 1. The key new feature is a controller, which employs a psychometric function incorporating a brightness regulator mechanism to improve the regions that are too dark or too bright. Our extended CBCE provides a better colored image under the specification of the Hubbard model provided by the AREDS2 Reading Center. The CBCE algorithm has two aims. Firstly, the shape parameters of the enhanced image are kept the same as those in the original in order to preserve the pathology of any retinal diseases. Secondly, the dynamic range of the image is improved by tuning scale parameters to make the retinal anatomical structure more visible.

A. Achromatic contrast sensitivity quality metric

In our CBCE algorithm, the image quality index is designed to select optimal GEV parameters. Our quality index was based on observations in a manner similar to human perception mechanisms, which are very sensitive to edges (or object boundaries) [21].

We utilized ACSQM index to objectively assess the perceived image quality of images. This was done by applying a psychometric function designed to accumulate the number of just-noticeable differences between the object and the background. For the color images, enhancement mechanisms of brightness, and contrast were quantified by computing the quality index on their luminance channel.

The results achieved by applying CSF to image processing to assess the perceptual quality of images has improved considerably over the last decade [29] [30] [31]. The purpose of using a CSF is to filter and extract the crucial anatomical structure information in the retinal images by weighting the spatial frequencies of the human visual stimuli. In our algorithm, the CSF model of Mannos and Sakrison [32] was adapted to modulate the enhanced images as follows:

$$\mathrm{CSF}(sf) \approx a(z + sf / f_0)\mathrm{e}^{-(sf / f_0)^d}, \qquad (12)$$

where a is a constant, z represents a zero frequency intercept controller, f_0 denotes the frequency constant for controlling the position of the central peak, d is a constant value to adjust the high frequency tail, and sf represents the spatial frequency. We utilized parameters in agreement with those reported by Mannos and Sakrison [32] to evaluate the retinal images. The parameters were a = 2.6, z = 0.0192, f_0 = 8.772 and d =1.1.

The CSF in (12) can be calculated in three steps for the frequency domain [19]. First, a Fast Fourier Transform (FFT) is applied to transform the luminance image into the spatial frequency domain, with the viewing distance approximately six times the image size. This provides a modulated frequency of about 5.625 cycles per degree. Second, the filtering operation is performed by multiplying the value returned by the Fourier transform to the CSF coefficient. Finally, an inverse Fast Fourier Transform (IFFT) is used to transform the spatial frequency coefficients back to the spatial domain. The calculated CSF luminance image is illustrated in Fig. 3(b).

The CSF luminance image was used to formulate the psychometric function, *pr*, to obtain a local visibility brightness contrast, $v_{local}(i)$, given by:

$$v_{local}(i) = pr(s_i, \mu_0, \sigma_0), \quad (13)$$

where s_i represents an edge strength at the *i-th* sliding window, which is derived from the standard deviation of the CSF luminance image in a window of 5×5 pixels. The edgeness result is shown in Fig. 3(c), and is employed to assess the edge-based contrast measurement. μ_0 and σ_0 denote the average and standard deviation of the edge strength of the original input image. Fig. 3(d) shows the local visibility brightness contrast image obtained from (13) which is used to predict the quality of the image.

A well-known psychometric function, Galton's ogive, can be employed to model the detection probability of the signal strength. This was introduced by Barten [16], in the form of a cumulative Gaussian distribution:

$$pr(s_i, \mu_0, \sigma_0) = \frac{1}{\sigma_0\sqrt{2\pi}} \int_{-\infty}^{s_i} \exp\left[-\frac{(x-\mu_0)^2}{2{\sigma_0}^2}\right] dx, \quad (14)$$

where *x* is an integration variable.

The edge-based contrast quality, q_e, is obtained by averaging the values, $v_{local}(i)$. It is employed on the edge strength to measure the contrast image, expressed as:

$$q_e = \frac{1}{N}\sum_{i=1}^{N} v_{local}(i). \quad (15)$$

As the index q_e approaches 1, our algorithm provides the maximum contrast.

Our investigation of the STARE and DIARETDB0 datasets revealed that most images had some regions that were too dark or too bright, caused by non-uniform illumination or media opacity. For example, the white area on the left of the image in Fig. 4(c) means that the corresponding region in the image in Fig. 4(a) is too dark. On the other hand, the white area in Fig. 4(d) shows that the corresponding region of the image in Fig. 4(b) is too bright. This problem can obscure the anatomical structures of the retina, and make some of the details necessary for a diagnosis undetectable. In our scheme, a brightness regulator maintains the inappropriate brightness identified by the proportions of the regions that are too dark or too bright, which is formulated as *PD*:

$$PD = \left(\sum_{r=1}^{m}\sum_{c=1}^{n} D(r,c)\right) \Big/ (m \times n), \quad (16)$$

where *m* and *n* are the image dimensions, and *D*(*r*, *c*) denotes a binary image that highlights the too dark or too bright regions.

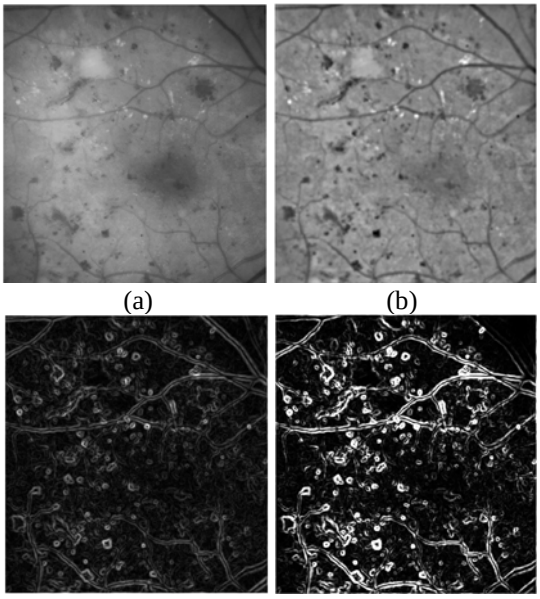

(a) (b) (c) (d)

Fig. 3 Output examples during the ACSQM process. (a) The luminance image of the input fundus image (file: Image109.png). (b) The CSF luminance image. (c) The edge strength of the CSF luminance image. (d) The local visibility brightness contrast after the processing of the psychometric function using (13).

In our scheme, regions with very low color variation are defined as having inappropriate brightness. From our experiments with the datasets, *D*(*r*, *c*) can be defined as:

$$D(r,c) = \begin{cases} 1, \ if \ S(RGB(r,c)) \le T, \\ 0, \ otherwise, \end{cases} \quad (17)$$

where *T* denotes the threshold value determined by Otsu's method [33]. *S*(*RGB*(*r*, *c*)) denotes the standard deviation at a pixel coordinate (*r*, *c*) formulated from the color variation in the RGB channels. *S*(*RGB*(*r*, *c*)) can be formulated as:

$$S(RGB(r,c)) = \sqrt{[(R(r,c)-M(r,c))^2 + (G(r,c)-M(r,c))^2 + (B(r,c)-M(r,c))^2]/3} \quad (18)$$

where *R*(*r*, *c*), *G*(*r*, *c*), and *B*(*r*, *c*) are the pixel values at the *r-th* row and the *c-th* column of the RGB channels. *M*(*r*, *c*) represents the luminance, which may be estimated by combining equal weights for each channel (as in a hue-saturation-intensity color model), or by using unequal weights (as in an XYZ color model) [19]. Our method represents *M*(*r*, *c*) using the mean values of the RGB channels at the (*r*, *c*) position. Our approach means that increasing the scale parameters will expand the dynamic range of the brightness of the red-green plane. However, expanding the direction to the dark or bright zones could increase the proportion of unsuitable areas. In that case, the proportions of unsuitable areas will decrease the edge-based contrast quality in order to avoid spurious optimal parameters. Hence, the factor *PD* is used to modify the quality index in (15).

The achromatic contrast sensitivity quality metric, q, is:

$$q = q_e - PD . \quad (19)$$

The compensation mechanism for the brightness regulator is illustrated in Fig. 5. Fig. 5(c) and (d) show two of the enhanced images which occurred during the tuning process. In Fig. 5(c), q_e = 0.8248 and PD = 0.0995, giving a quality index, q, of 0.7253. In Fig. 5(d), q_e = 0.8193 and PD = 0.0309, giving a quality index, q = 0.7884. These results mean that the enhanced image in Fig. 5(d) will be selected as the output image, because it has a smaller unsuitable area, especially on the right hand side.

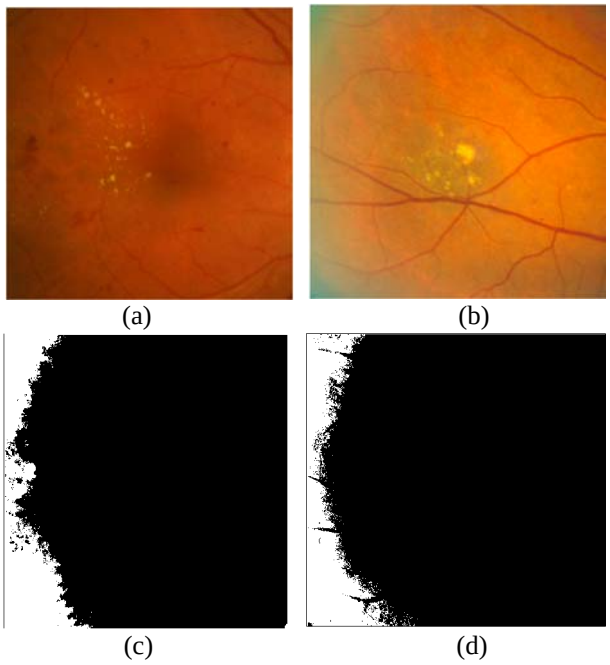

Fig. 4 Binary images showing the regions that are too dark or bright using the Otsu threshold.
(a) Image from files Image015.png. (b) Image from files Im0307.ppm. (c) Binary image representing the dark regions of image (a). (d) Binary image representing the bright regions of image (b).

B. Color balance and contrast enhancement (CBCE)

Our CBCE algorithm adjusts the brightness, contrast, and color balance of color retinal images. It was developed from the HS-GEV using ACSQM and a brightness regulator to tune the GEV parameters. The algorithm, shown in outline in Fig. 2, can be described in three steps. To help with the description, we will refer to the processing of the color retinal image in Fig. 5(a), which was cropped to the region of interest in the macular area.

The first step sets RGB color space variables by following the color retinal image specifications of Hubbard *et al*. [3]. The parameters consist of brightness, contrast, and color balance. The brightness values for the color bands, b = {*R*, *G*, *B*} are bv_b = {192, 96, 32}. The lower bound, lb_b, and upper bound, ub_b, for each color band, b, are [$lb_{b=R}$, $ub_{b=R}$] = [112, 240], [$lb_{b=G}$, $ub_{b=G}$] = [16, 144] and [$lb_{b=B}$, $ub_{b=B}$] = [16, 48]. These parameters are employed to tune the transfer functions of each color channel, which adjust the color balance and image contrast.

The second step estimates the GEV parameters for each color channel. The cropped input image is resampled by reducing its size to 64×64 pixels by the nearest neighborhood method [19]. The down-sampled data is used to estimate three parameters: shape, location**,** and scale ($\hat{\kappa}_b$, $\hat{\mu}_b$, and $\hat{\sigma}_b$) for each color band, b, by using PWMs. From the red channel in Fig. 5(a), the three parameters are $\hat{\kappa}_{b=R}$ =0.41, $\hat{\sigma}_{b=R}$ =22.73, and $\hat{\mu}_{b=R}$ = 197.14. The first moment, b_0 = 203.47, of (11) represents the mean value, which deviates from the specified brightness of the red channel, $bv_{b=R}$, which is 192.

To adjust the color balance of each color channel, the new location parameters, $\hat{\mu}_b'$ are calculated by replacing the first moment, b_0, in (10) with the specified brightness value, bv_b, as given by:

$$\hat{\mu}_b' = bv_b - \frac{\hat{\sigma}_b}{\hat{\kappa}_b}\left[1 - \Gamma\left(1 + \hat{\kappa}_b\right)\right]. \quad (20)$$

In the case of Fig. 5(a), bv_b, $\hat{\sigma}_b$, and $\hat{\kappa}_b$ in (20) are replaced with $bv_{b=R}$ =192, $\hat{\sigma}_{b=R}$ =22.73, and $\hat{\kappa}_{b=R}$ =0.41. The new location parameter of the red band, $\hat{\mu}_{b=R}'$ =185.67, provides a new intensity range, $0 < x \le 241.72$.

Next, the scale parameter of each color channel is used to redistribute the intensity values, x, to the new ranges. In our study, the input data scale parameters correspond approximately to the shape parameters, which are classified into four cases.

Case 1: $-0.2 \le \hat{\kappa}_b \le 0.2$. In this case, the image data distribution approaches a Type I GEV function in (4). The probability of the intensity values, x, covers most of the data range [24], $p(\mu_b - 2\sigma_b \le x \le \mu_b + 7\sigma_b) = 0.99$. In the model of Hubbard *et al*. [3], 256 intensity levels were divided into 16 scales, and the brightness values of the red channel were distributed in the ranges [7/16, 15/16], [1/16, 9/16] for the green channel, and [1/16, 3/16] for the blue channel. The intensity values, such as those for the red and green channels, can be redistributed within their specified boundary limits. Therefore, the scale parameters for each color channel can be approximated from the probability confidence interval; for instance, those for the red and green channels are given by:

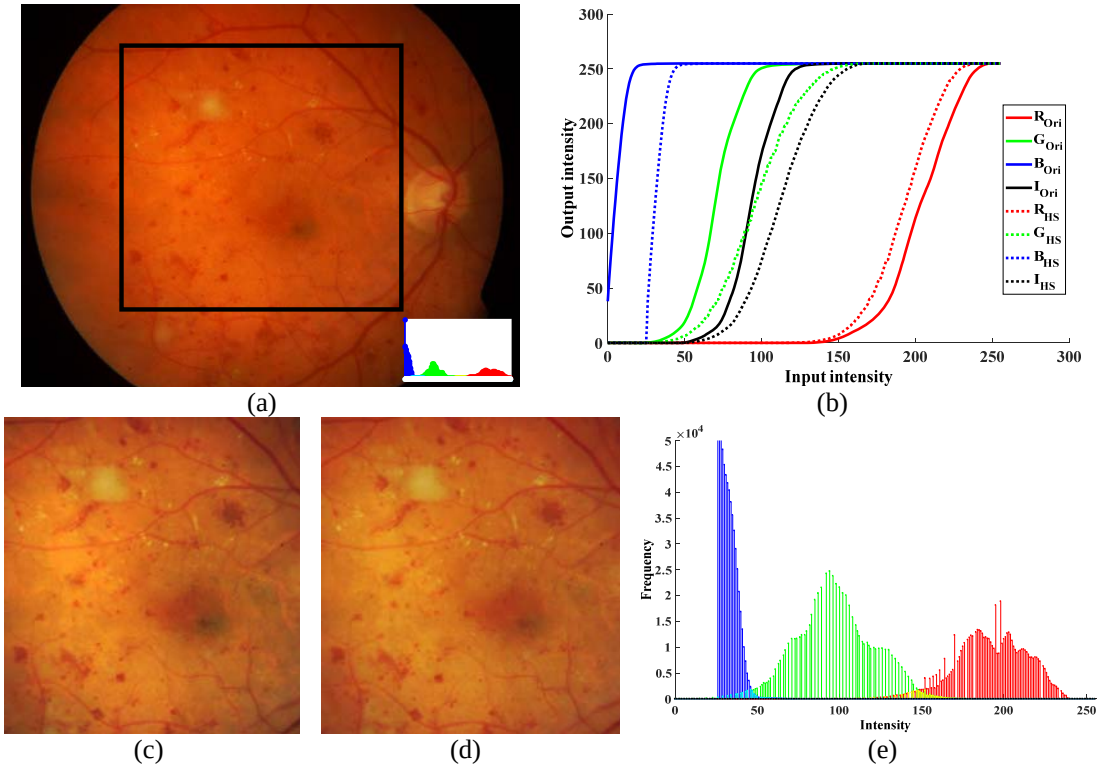

Fig. 5 Color retinal image enhancement.
(a) Input fundus image (file: Image109.png), (b) Tone mapping curves of R, G, B, and L (solid lines), (c) The output image with q_e = 0.8248 and PD = 0.0995, (d) The highest Q for the output image with q_e = 0.8193 and PD = 0.0309, (e) Histogram of the R, G, and B channels.

$$(\hat{\mu}_b' + 7\hat{\sigma}_b') - (\hat{\mu}_b' - 2\hat{\sigma}_b') = 128, \quad (21)$$

which gives $\hat{\sigma}_b' \approx 14.22$.

The scale parameters in cases 2 and 3 can be determined by the range of the random variable, x, in (5). Hosking [25] recommended equating x to $\mu + \sigma/\kappa$:

$$x = (\hat{\mu}_b' + \hat{\sigma}_b') / \hat{\kappa}_b . \quad (22)$$

To obtain a good point estimation, the shape parameters should be within the range -½ < $\hat{\kappa}$ < ½ [24]. Thus, cases 2 and 3 can be formulated as follows:

Case 2: $-0.5 < \hat{\kappa}_b < -0.2$. This is a Type III GEV distribution. From (4) and (22), the scale parameters can be estimated from the lower bound of the brightness values, lb_b of each color channel.

$$\hat{\sigma}_b' = \hat{\kappa}_b . lb_b - \hat{\mu}_b' . \quad (23)$$

Case 3: $0.2 < \hat{\kappa}_b < 0.5$. The scale parameters in this case are GEV type II. From (4) and (22), they can be approximated from the upper bound of the brightness values, ub_b, of each color channel.

$$\hat{\sigma}_b' = \hat{\kappa}_b . ub_b - \hat{\mu}_b' . \quad (24)$$

Case 4: $\hat{\kappa}_b \le -0.5$ or $\hat{\kappa}_b \ge 0.5$. This case usually occurs when the intensity of the red channel of the retinal image lies above the saturation point. The scale parameters can be obtained from PWM estimation in the first step without alteration.

During the tuning process, the scale parameters of the four cases are estimated by searching the optimal scale values to redistribute the intensity values within the tolerance interval $[\hat{\sigma}_b' - 5,\ \hat{\sigma}_b' + 10]$. From the tolerance interval, a linear scale is used to determine 32 candidates for the scale parameters from the combination of the red and green bands. They are $\{\hat{\sigma}_{b=R}'^{(j)}\} = \{\hat{\sigma}_{b=R}' - 5, \hat{\sigma}_{b=R}' - 4, ..., \hat{\sigma}_{b=R}' + 9, \hat{\sigma}_{b=R}' + 10\}$ for the red, and $\{\hat{\sigma}_{b=G}'^{(k)}\} = \{\hat{\sigma}_{b=G}' - 5, \hat{\sigma}_{b=G}' - 4, ..., \hat{\sigma}_{b=G}' + 9, \hat{\sigma}_{b=G}' + 10\}$ for the green channels, where index j and k = 1, 2, 3 … 16. All the candidate scales in the two sets will be employed to enhance the image in the next step**.**

In the third step, the optimal GEV parameters in the red and green channels are determined by iterative probes with the candidate scales which redistribute the brightness values in the specified dynamic ranges. In our algorithm, the blue channel is translated only to the specified brightness, because the intensity in this channel does not contain much information related to the retina, and is usually distributed in a narrow interval.

An exhaustive search of combinations of candidate scales in $\{\hat{\sigma}_{b=R}'^{(j)}\}$ and $\{\hat{\sigma}_{b=G}'^{(k)}\}$ is employed to find the optimal GEV parameters. The outer loop operates over the red channel, and the inner loop over the green channel. These loops are indexed by two parameters, j and k, where j is used to iterate the j^{th}

scale in $\{\hat{\sigma}'_{b=R}{}^{(j)}\}$, and index k is used to iterate the k^{th} scale in $\{\hat{\sigma}'_{b=G}{}^{(k)}\}$. For each iteration of the loop, the candidate scales perturbs the location parameters in (20), and then the transfer function in (7) redistributes the grey levels. Then, the ACSQM evaluates the quality index of the enhanced image, and the optimal GEV parameters are chosen from the maximum quality index, q.

The output image, g, in Fig. 5(d) was obtained with the adjusted mean values of the R, G, and B channels, bv_b={192.46, 96.86, 32.18}. The original and the optimal GEV parameters are shown in Table I. The optimal transfer functions for the color channels are shown in Fig. 5(b), which also includes the luminance (L) with its CDF from the original image (the solid line). The output image histograms of each color channel are shown in Fig. 5(e).

TABLE I: GEV parameters of the retinal image in Fig. 5.

Parameters	Original image (R,G,B)	Enhanced image (R,G,B)
Shape	(0.41, 0.27, -0.01)	(0.40, 0.26, -0.01)
Scale	(22.73, 14.14, 4.10)	(23.01, 19.19, 4.10)
Location	(197.14, 65.53, 3.75)	(186.20, 89.68, 29.75)

IV. Results and Discussion

The retinal image data sets were used to evaluate and compare our method with other methods that enhance color retinal images, such as HS-GEV [7], normalized convolution and noise removal (NCNR) [5], and color retinal image enhancement based on luminosity and contrast adjustment (LCA) [6].

We consider that the output images have improved quality if they provide good image detail, good contrast, and color balance, which enables them to be of increased usefulness to ophthalmologists. However, color image assessment is not easy to evaluate using only quantitative measurements. To determine if an image has good quality requires both quantitative and visual assessment. The quantitative methods used for objective assessment are quaternion structural similarity (QSSIM) [34], measured colorfulness ($M^{(3)}$) [35], lightness order error (LOE) [36], and the global contrast factor (GCF) [37], which can be categorized into two groups.

The first quantitative assessment group consists of QSSIM and $M^{(3)}$ assess color quality. QSSIM measures luminance, chrominance, or the combined degradation between a reference and enhanced image [34]. In our case, there is no reference retinal image, so the input image was employed. This is less ideal for image quality assessment, but it allows us to judge how well the enhancement method preserves the structure of the achromatic and chromatic information. As a consequence, the highest QSSIM score of 1 means that the enhancement method completely preserved the structural image.

Unlike QSSIM, $M^{(3)}$ is able to evaluate colorfulness without a reference image, and utilizes the opponent color space, which works well with color retinal images. Moreover, $M^{(3)}$ has the highest correlation with the psychophysical experiments of Hasler and Susstrunk [35]. Their seven scores, {0, 15, 33, 45, 59, 82, 109}, correspond to {not colorful, slightly colorful, moderately colorful, averagely colorful, quite colorful, highly colorful, extremely colorful}.

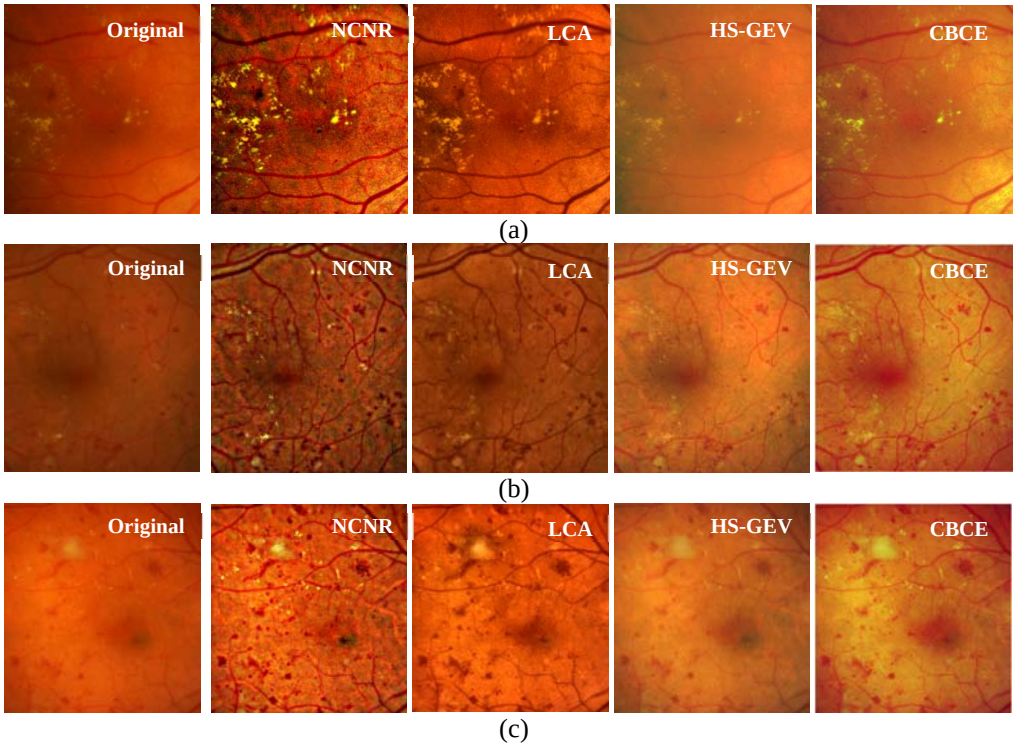

Fig. 6: Enhancement result comparisons.
(a), (b), (c) Image007.png, Image101.png, and Image109.png from DiaretDB0.

The second quantitative method group uses LOE to assess lightness order, and GCF for edge contrast. LOE can measure naturalness preservation based on the relative lightness order difference between the original and enhanced images [36]. A smaller LOE value means that the retinal enhancement better preserves the lightness order. GCF employs image contrasts at various resolution levels to measure the richness of detail in the green channel [37]. It also does not require a reference image.

Visual assessments are shown in Fig. 6 and 7, with the images coming from DiaretDB0 and STARE. The original images in the first column exhibit a range of image qualities based on their degree of illumination, contrast, and color balance. The last 4 columns show the enhanced images using the NCNR, LCA, HS-GEV, and CBCE methods, respectively.

The color balance for the images was modelled by Hubbard *et al.* [3] who specified it with the R, G, and B brightness set to 192, 96, and 32, which resulted in color ratios of G/R = 0.5 and B/R = 0.17. As seen from the enhanced results in Fig. 6 and 7, and the experimental results in the third and the fourth column of Table II, our method and HS-GEV improved the Hubbard's color-ratios better than NCNR, and LCA.

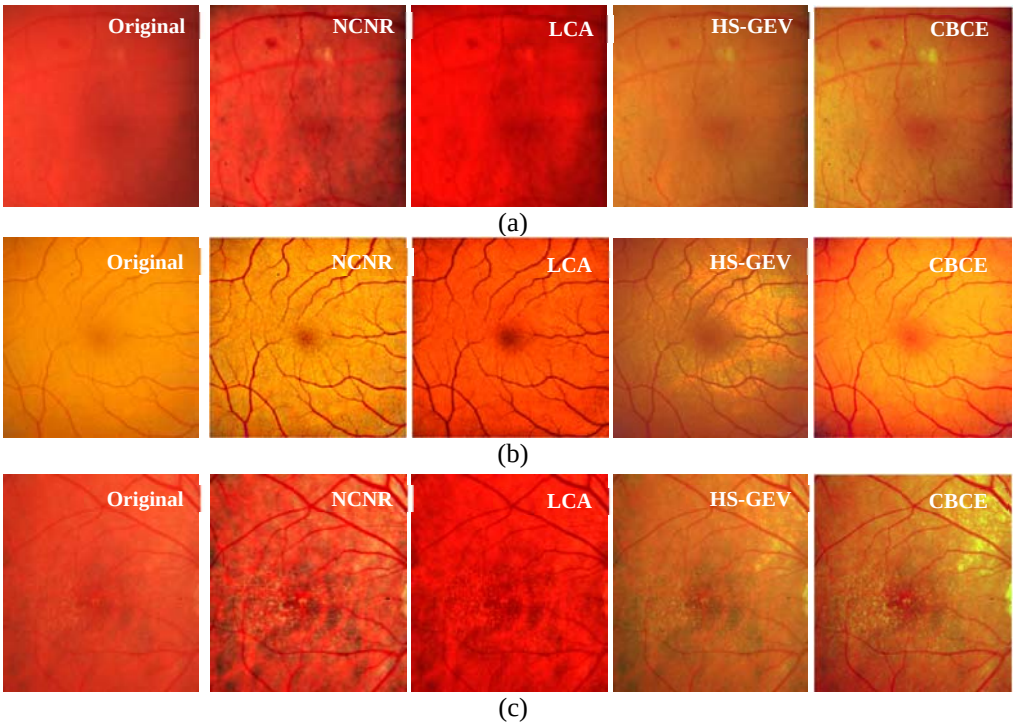

Fig. 7: Enhancement result comparisons.
(a), (b), (c), Im0013.ppm, Im0082.ppm, and Im0039.ppm from STARE.

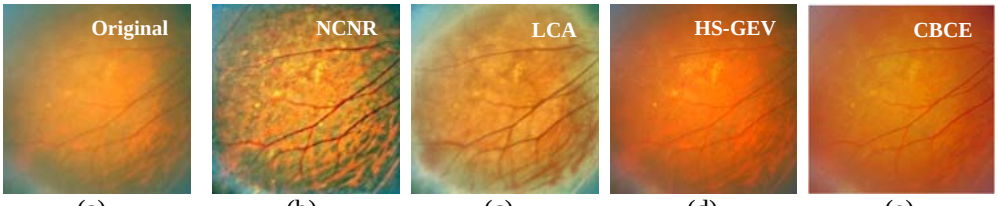

Fig. 8: Comparison of improvements in the color cast of the retinal enhancement algorithms applied to Im0292.ppm.
(a) Original image, (b) Output using NCNR, (c) Output using LCA, (d) Output using HS-GEV, (e) Output using our method, CBCE.

Fig. 8 shows the dark areas generated by each method. Our method improved the quality of the dark regions, while HS-GEV, NCNR, and LCA enhanced the image around the macular area but the corner areas remained dim. This indicates that our method improved the non-uniform illumination and reduced the regions that were too dark.

Our method provides colorfulness scores in the range of 70 to 80, which are lower than NCNR, as seen from the $M^{(3)}$ values in Table II. Nevertheless, in the case of images with uneven luminance, as in Fig. 9, our method and HS-GEV produce significantly better colorfulness.

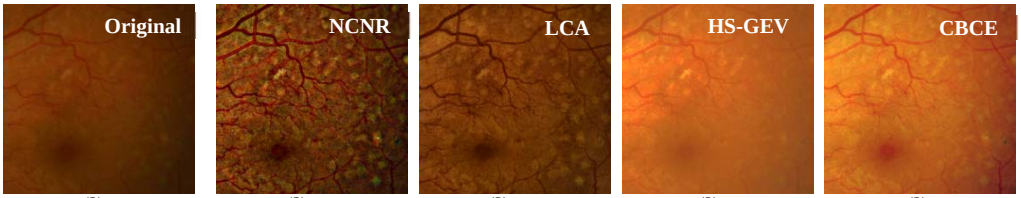

(a) $M^{(3)}$=46.20 (b) $M^{(3)}$= 55.75 (c) $M^{(3)}$= 44.03 (d) $M^{(3)}$=68.98 (e) $M^{(3)}$=72.29

Fig. 9: Colorfulness comparison of algorithms applied to Image039.png.
(a) Original image, (b) Output using NCNR, (c) Output using LCA, (d) Output using HS-GEV, (e) Output using our method, CBCE.

.

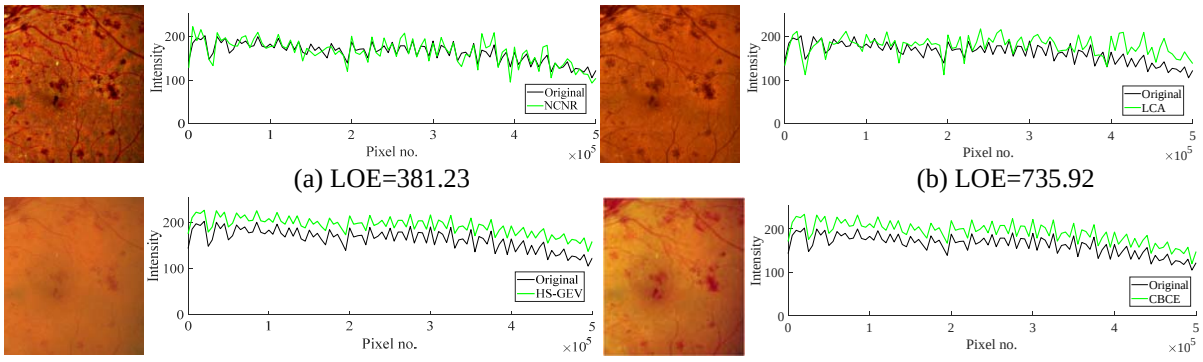

(a) LOE=381.23 (b) LOE=735.92

(c) LOE=13.86 (d) LOE=7.98

Fig. 10: Output image and graph showing the lightness in each pixel between Image032.png and the output image.
(a) Output using NCNR, (b) Output using LCA, (c) Output using HS-GEV, (d) Output using our method, CBCE.

Fig. 10 shows the relative lightness order, which is utilized to quantitatively evaluate naturalness preservation. The data on the x-axis and y-axis represent the pixel number in the image and the maximum intensity values of the three color channels, respectively. The graphs in Fig. 10 plot every pixel of the image. The black line represents the input image lightness, whereas the green line represents the output image lightness. Our algorithm preserves the relative lightness order, outperforming NCNR, LCA, and HS-GEV. The LOE measure [36] judges the similarity in lightness relative order between the input and output image, with a smaller LOE value meaning they are more similar. Fig. 10 shows that the NCNR and LCA black lines are quite different from the green line, and so have a bigger LOE.

Table II summarizes the objective comparison results of our method with other image enhancement methods for STARE and DiaretDB0. The comparison results were calculated with 83 STARE images and 130 DiaretDB0 images. The last 6 columns give the mean and standard deviation of the color ratios, $M^{(3)}$, GCF, QSSIM, and LOE in each quantitative method.

Our method has as good a color balance as HS-GEV, achieving optimum green to red color balance ratios while HS-GEV is better for blue-to-red ratios. Although HS-GEV is better for blue-to-red ratios, this is less important since the information included in the green channel is richer than for blue. The average green-to-red and blue-to-red color balance ratios (Mean ± SD) of our method are 0.505±0.002 and 0.166±0.002, and HS-GEV's ratios are 0.516±0.093 and 0.171±0.030, which is close to the color balance specification from the Hubbard model.

HS-GEV yields the highest QSSIM scores, averaging 0.91±0.09, while our method is in second place, which indicates that both methods can preserve structural similarity from the input images. Although our method cannot preserve structural similarity as well as HS-GEV, the visual assessment in Fig. 6 and 7 show that our method provides better visibility of the retinal anatomical structures than HS-GEV.

NCNR gives the highest $M^{(3)}$ scores, averaging 74.53±17.01. Our method employs GEV's scale parameters to spread the dynamic range between the boundary limits specified by Hubbard's model. This means that our method provides a colorfulness scores in the range 70 to 80, as seen from the $M^{(3)}$ values in Table II. However, for uneven luminance images, our method has the highest colorfulness scores compared to the other methods, as shown in Fig. 9.

NCNR gives the highest GCF score, 5.13±1.12. Within the boundary limits, HS-GEV and our method gives lower GCF values compared to NCNR. Although our method cannot perform image contrast as well as NCNR, the visual assessment in Fig. 6 and 7 show that NCNR could generate dark blood vessels or dark regions, while our method gives more visually pleasing results. Furthermore, our method

confirms the GCF assumption because it provides GCF values higher than HS-GEV for most of the input images.

As seen from the experimental results in Table II, there exists a trade-off between QSSIM, GCF, and $M^{(3)}$ indexes The more contrast and colorfulness value, the fewer structural similarity value. In contrast, the more structural similarity value, the fewer contrast and colorfulness value. Although our method could not reaches the highest in QSSIM, GCF, and $M^{(3)}$ value but the visual assessment in Fig. 6 and 7 show that our method could deal with this trade-off problem and give a more visually pleasing results when compared to other methods.

Our method gives the lowest quantitative measure for LOE (18.17±14.82), which confirms the naturalness preservation. This indicates that our method performs better than other methods in preserving the relative lightness order.

In summary, compared with other approaches, our method not only enhances the contrast of anatomical details, but also maintains the structural similarity and the naturalness of the retinal images.

TABLE II: Performance of various methods on the DIARETDB0 and STARE datasets

Method	Dataset	G/R	B/R	$M^{(3)}$	GCF	QSSIM	LOE
NCNR	DIARETDB0	0.390±0.055	0.097±0.047	70.77±13.80	4.78±0.80	0.59±0.05	366.14±101.23
	STARE	0.591±0.176	0.265±0.219	89.38±20.29	3.97±1.25	0.72±0.06	266.74±98.30
	Both	0.431±0.123	0.131±0.123	74.53±17.01	4.62±0.96	0.61±0.07	346.01±108.04
LCA	DIARETDB0	0.389±0.057	0.072±0.047	58.02±13.60	2.38±0.49	0.82±0.04	663.36±188.01
	STARE	0.343±0.262	0.120±0.314	94.52±20.30	3.76±1.11	0.78±0.06	585.55±287.67
	Both	0.380±0.129	0.082±0.147	65.41±21.10	2.66±0.86	0.81±0.05	647.60±213.23
HS-GEV	DIARETDB0	0.519±0.104	0.172±0.034	63.33±7.39	0.78±0.47	0.91±0.10	21.85±45.62
	STARE	0.502±0.003	0.168±0.003	77.31±10.92	2.46±0.45	0.93±0.03	35.54±33.14
	Both	0.516±0.093	0.171±0.030	66.16±9.94	1.12±0.82	0.91±0.09	24.62±43.64
CBCE (Our method)	DIARETDB0	0.506±0.002	0.166±0.002	72.05±3.54	2.66±0.51	0.85±0.10	15.41±5.44
	STARE	0.503±0.003	0.168±0.002	79.32±11.12	2.78±0.80	0.96±0.02	29.03±28.98
	Both	0.505±0.002	0.166±0.002	73.52±6.56	2.69±0.58	0.87±0.10	18.17±14.82

V. Conclusions and Future Work

Our color retinal image enhancement method (CBCE), based on the histogram specification, was presented in this paper. The brightness, contrast, and color balance of retinal images were automatically improved by using HS transfer functions based on a GEV distribution. The GEV parameters were designed with Hubbard's model to specify the color retinal images in order to improve the image quality. The transfer function was tuned by a psychometric index based on an edge-based contrast measurement and a contrast sensitivity function. To compensate for non-uniform illumination of the retinal images, the index value was modified with too dark and too bright regions named as ACSQM. Our CBCE method was tested on retinal images from the STARE and DIARETDB0 databases. The proposed method achieves our contributions for improving the image quality as seen from Figs. 6 and 7 that obtain good color balance and better color contrast than other approaches. Additionally, work can be done such as improving color contrast by increasing colorfulness to reveal hidden information in the fundus photographs and large scale clinical testing to declare the enhanced results as sub-standard for screening the image quality.

References

[1] S. L. Fine, J. W. Berger, M. G. Maguire and A. C. Ho, "Agerelated macular degeneration," *New Engl J Med*, vol. 342, no. 7, p. 483492, 2000.

[2] L. P. Aiello, T. W. Gardner, G. L. King, G. Blankenship, J. D. Cavallerano, F. L. 3. Ferris and R. Klein, "Diabetic retinopathy," *Diabetes Care*, vol. 21, no. 1, pp. 143-156, 1998.

[3] L. D. Hubbard, R. P. Danis, M. W. Neider, H. D. Thayer, H. D. Wabers, J. K. White, A. J. pugliese and m. F. Pugliese, "Brightness, contrast, and color balance of digital versus film retinal Images in the age-related eye disease study 2," *Journal of Investigative Ophthalmology & Visual Science*, vol. 49, no. 8, pp. 3269-3282, 2008.

[4] L. D. Hubbard, "Digital color fundus image quality: the impact of tonal resolution," Spring/2009 Vol 31:1 p.15. [Online]. Available: http://www.opsweb.org/?page=crareference. [Accessed 16 June 2015].

[5] D. Peishan, S. Hanwei, Z. Jianmei, L. Ling, W. Jing and F. Min, "Retinal fundus image enhancement using the normalized convolution and noise removing," *International Journal of Biomedical Imaging*, pp. 1-13, 2016.

[6] Z. Mei, J. Kai, W. Shaoze, Y. Juan and Q. Dahong, "Color retinal image enhancement based on luminosity and contrast adjustment," *IEEE Rev. Biomed. Eng.*, no. 99, pp. 1-7, 2017.

[7] S. Intajag, S. Kansomkeat and P. bhurayanontachai, "Histogram specification with generalized extreme value distribution to enhance retinal images," *IET Electronics Letters*, vol. 52, no. 8, pp. 596-598, April 2016.

[8] E. S. L. Gastal and M. M. Oliveira, "Domain transform for edge-aware image and video processing," *ACM Trans. on Graphics*, vol. 30, no. 4, p. 1244–1259, 2011.

[9] J. Rajan, K. Kannan and M. R. Kaimal, "An improved hybrid model for molecular image denoising," *J. of Math. Imaging and Vision,* vol. 31, no. 1, p. 73–79, 2008.

[10] A. B. Hamza, P. L. Luque-Escamilla, J. Martınez-Aroza and R. Roman-Roldan, "Removing noise and preserving details with relaxed median filters," *J. of Math. Imaging and Vision,* vol. 11, no. 2, p. 161–177, 1999.

[11] C. Wang and Z. Ye, "Brightness preserving histogram equalization with maximum entropy: a variational perspective," *IEEE Trans. Consum. Electron.,* vol. 51, no. 4, p. 1326–1334, 2005.

[12] H. Ibrahim and N. Kong, "Brightness preserving dynamic histogram equalization for image contrast enhancement," *IEEE Trans. Consum. Electron.,* vol. 53, p. 1752–1758, 2007.

[13] D. Sheet, H. Garud, A. Suveer, M. Mahadevappa and J. Chatterjee, "Brightness preserving dynamic fuzzy histogram equalization," *IEEE Trans. Consum. Electron,* vol. 56, no. 4, pp. 2475-2480, 2010.

[14] T. Jintasuttisak and S. Intajag, "Color retinal image enhancement by raleigh contrast limited adaptive histogram equaliztion," *Proc. Int. Conf. ICCAS*, pp. 692-687, 2014.

[15] K. Zuiderveld, Contrast limited adaptive histogram equalization, San Diego: Academic press professional, pp.474-485, 1994.

[16] G. J. P. Barten, Contrast sensitivity of the human eye and its effects on image quality, Washington, DC: SPILE, 1999.

[17] A. Hoover, V. Kouznetsova and M. Goldbaum, "Locationg blood vessels in retinal images by piecewise threshold probing of a matched filter response," *IEEE Trans. Med. Imag,* vol. 19, no. 3, pp. 203-210, 2000.

[18] T. Kauppi, V. Kalesnykiene, J. K. Kammarainen, L. Lensu, L. Sorri, H. Uusitalo and H. Kalviainen, "DIARETDB0 : Evaluation database and methodology for diabetic retinopathy algorithms," in *Technical report*, Lappeenranta, finland, 2006.

[19] C. R. Gonzalez and E. R. Woods, Digital image processing, 3rd edn., Pearson, 2009.

[20] D. Coltuc, P. Bolon and J. M. Chassery, "Exact histogram specification," *IEEE Trans. Image Process.,* vol. 15, no. 5, pp. 1143-1152, 2006.

[21] W. K. Pratt, Digital image processing, 4th edn., New York, United States: John wiley & Sons Inc, 2007.

[22] R. A. Fisher and L. H. C. Tippett, "Limiting forms of the frequency distribution of the largest or smallest member of a sample," *Proc. of Cambridge Philosophical Society*, vol. 24, pp. 180-290, 1928.

[23] T. Fararo and R. Katz, "Extremes and design values in climatology," *World meteorological organization* , pp. WCAP-14, WMO/TD-No. 386., 1990.

[24] S. Kotz and S. Nadarajah, Extreme values distributions: theory and applications, Covent Garden, London: Imperial College Press, 2000.

[25] J. M. Hosking, J. R. Wallis and E. F. Wood, "Estimation of the generalized extreme-value distribution by the method of probability weighted moments," *Technometreics,* vol. 27, no. 3, pp. 251-161, 1985.

[26] E. Castillo, S. A. Hadi, N. Balakrisnan and M. J. Sarabia, Extreme value and related models with applications in engineering and science, New York: John Wiley & Sons, 2004.

[27] K. A. Jain, Fundamentals of digital image processing, Englewood Cliffs NJ: Pentice-Hall, Inc, 1989.

[28] S. Kullback and R. A. Leibler, "On information and sufficiency," *Ann. Math. Stat.,* vol. 22, no. 1, p. 79–86, 1951.

[29] S. Wang, K. Jin, H. Lu, C. Cheng, J. Ye and D. Qian, "Human visual system-based fundus image quality assessment of portable fundus Camera photographs," *IEEE Trans. Med. Imag.,* vol. 35, no. 4, pp. 1046-1055, 2016.

[30] G. Ginesu, F. Massidda and D. D. Giusto, "A multi-factors approach for image quality assessment based on a human visual system model," *Signal Process, Image Commumn,* vol. 21, no. 4, pp. 316-333, 2006.

[31] Y. Han and y. Cai, "Contrast sensitivity function calibration based on image quality prediction," *Opt. Eng.,* vol. 53, no. 11, p. 113107, 2014.

[32] J. L. Mannos and D. J. Sakrison, "The effects of a visual fidelity criterion on the encoding of images," *IEEE Trans. Inf. Theory,* vol. 20, no. 4, pp. 525-536, 1974.

[33] N. Otsu, "A threshold selection method from gray-level histogram," *IEEE Trans. Syst. Man, Cybern,* Vols. SMC-9, no. 1, pp. 62-66, 1979.

[34] A. Kolaman and O. Pecht, "Quaternion structural similarity a new quality index for color images," *IEEE Trans. Image Process.,* vol. 21, no. 4, p. 1526 – 1536, 2012.

[35] D. Hasler and S. Susstrunk, "Measuring colorfulness in natural images," *Proc. SPIE,* vol. 5007, pp. 87-95, 2003.

[36] S. Wang, J. Zheng, H. Hu and B. Li, "Naturalness preserved enhancement algorithm for non-uniform illumination images," *Trans. Image Process.,* vol. 22, no. 9, pp. 60-70, 2013.

[37] K. Matkovic, L. Neumann, A. Neumann, T. Psik and W. Purgathofer, "Global Contrast Factor - a New Approach to Image Contrast," in *Computational Aesthetics in Graphics, Visualization and Imaging*, Girona, Spain, May, 2005, 159-167.